PAPER 26

Beneficiation of Concentrated Ultrafine Suspensions with a Falcon UF concentrator

Jean-Sébastien Kroll-Rabotin[1], Florent Bourgeois[1], Éric Climent[2]

[1]Université de Toulouse,
Laboratoire de Génie Chimique
Toulouse, France

[2]Université de Toulouse,
Institut de Mécanique des Fluides de Toulouse,
Toulouse, France

Key Words: Centrifugal, gravity, concentration, Falcon UF, modeling

43rd Annual Meeting of the
Canadian Mineral Processors

January 18 to 20, 2011
Ottawa, Ontario, Canada

ABSTRACT

Falcon concentrators are enhanced gravity separators designed for concentrating fine and ultrafine slurries. The Falcon UF model is unique in that it is dedicated to beneficiation of ultrafines, one key feature being that it does not make use of any fluidisation water. In a former study, we investigated the physical mechanisms that govern the transport of ultrafine particles (in the range 10 to 80 μm) inside Falcon UF concentrators, and concluded that separation efficiency is governed by differential settling. Initially, we derived and published a predictive model of the partition function under dilute conditions. The present paper proposes an extension of the initial model to concentrated ultrafine suspensions for application to industrial scenarios. The paper discusses how hindered settling has been added into the initial model to account for solid concentration effects. The modified model is tested against experiments carried out with a laboratory scale UF Falcon concentrator from dilute conditions up to 30 vol%. A good agreement between measurements and model predictions is obtained, which confirms that our hypotheses about the physics of separation inside a UF Falcon separator remain valid even at high concentrations.

INTRODUCTION

The Falcon concentrator is a fast spinning bowl that is fed at its centre of rotation. It uses centrifugal force to separate particles that are transported inside a thin liquid film that flows upward along the inclined wall of the bowl (McAlister and Armstrong, 1998). Due to differential settling, dense and coarse particles are concentrated inside the bowl whereas light and fine particles are rejected with the overflow stream. The fast rotation speed of the bowl yields high centrifugal force several hundred times the attraction of Earth. Despite the thinness of the liquid film (between 100 μm and 1 mm with a Falcon L40) where separation takes place, the Falcon concentrator can treat high flowrates (up to 30 L/min). At the bottom of the bowl, an impeller transmits the bowl rotation to the feed, which drains upward by centrifugal force as soon as it hits the base of the spinning bowl (Figure 1).

MODELLING THE UF FALCON CONCENTRATOR

In a previous article (Kroll-Rabotin et al., 2010), we justified that particle transport in the liquid film is the driving separation mechanism inside the UF Falcon. As a result, since ultrafine particle transport is dictated by the flow field, the separation that takes place inside a UF Falcon concentrator can be predicted by combining knowledge of the fluid flow field inside the flowing film with some hypotheses about particle capture based on observations by Deveau (2006).

Particle Transport Modelling

In our hydrodynamic model, particles are represented as point particles. From a purely theoretical viewpoint, this means our sedimentation-driven model is valid provided particles do not affect fluid flow and do not interact with each other. In practice, this implies that particles must be finer than film thickness. Since film thickness is a few hundred microns at the most, we expect that the theoretical domain of validity of our model extends to minus 100 micrometer

particles.

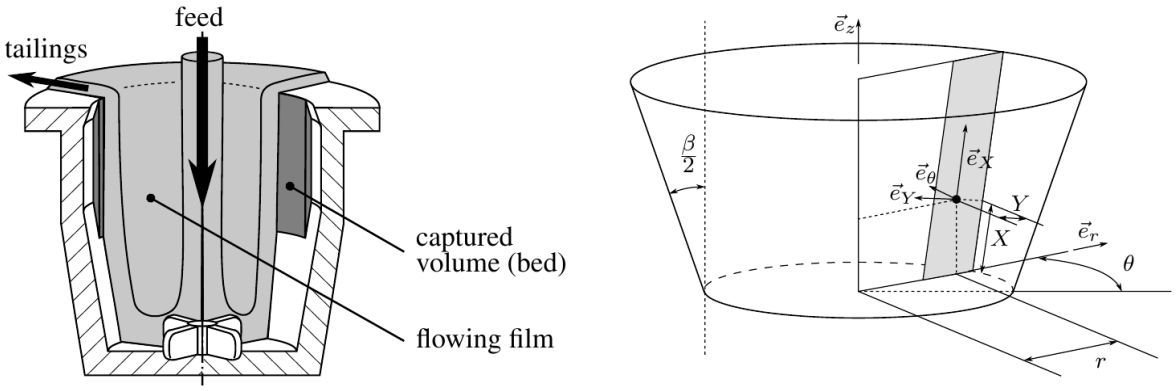

Figure 1: Schematics of the Falcon UF bowl and corresponding notations describing its geometry.

By studying the composition of the particle bed that forms on the bowl surface with ultrafine mineral suspensions in the 10 to 100 µm range, Deveau (Deveau and Young, 2005; Deveau, 2006) showed the presence of a higher grade concentrate at the surface of the bed. This observation means that the particle bed does not undergo significant rearrangement over time, otherwise light particles would tend to be driven out of the bed by denser particles, which would contradict Deveau's observations. This is consistent with our assumption that differential settling is the mechanism that governs separation of ultrafine particles in a UF Falcon concentrator. In addition, because of their low inertia, it is sound to assume that ultrafine particles that have been entrained in the bed cannot make their way out of the bed. In other words, resuspension of particles from the bed into the flowing film is negligible. In the end, our model assumes that every particle that reaches the surface of the bed that builds up on the bowl surface is trapped and reports to the concentrate.

Velocity Field Inside the Flowing Film

From visual observation made by removing the cover of the bowl during operation, it is obvious that film thickness is very small, say of the order of the thickness of a nail. We did however compute the flow over the conical wall of the Falcon L40 concentrator with direct numerical simulation (DNS) in order to assess the actual film thickness.

Figure 2 shows how single-phase DNS simulation was used to estimate film thickness. When the simulation domain is larger than the actual film thickness (500 microns in Figure 2), the fluid flow splits into two clearly distinct regions. In the region closest to the wall, the fluid has the same rotation speed u_y as the bowl. It is this rotation combined with the outward opening angle of the bowl that drains the fluid upward. Moving to the second region away from the wall (*i.e.* closer to rotation axis), the fluid velocity u_y in the direction parallel to the wall is null: the only non-null component of fluid velocity is solid body rotation, mind due at a slightly lower rotation rate than the bowl.

By differenciating these two zones based on their distinct flow regimes, it is possible to estimate

the thickness of the film. In Figure 2, the film actually corresponds to the thin zone close to the bowl surface with a non-zero flowrate. We decreased film thickness starting at 500 microns (see Figure 2), until we found only one flow regime throughout the film thickness. Figure 3 corresponds to such a condition, with a film thickness just below 200 microns. This thickness depends on operating conditions and 2 L/min and 1000 rpm were used to calculate Figure 2 and 3.

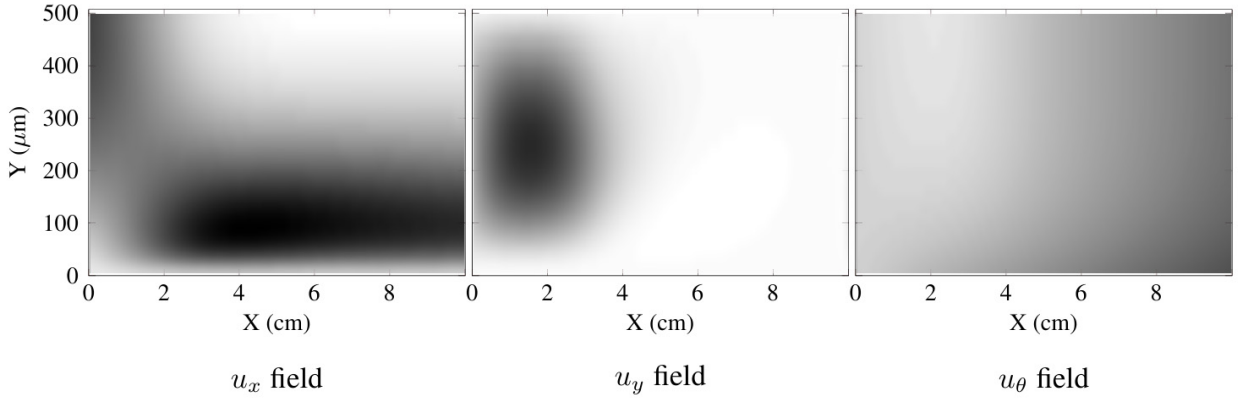

Figure 2: Flow field computed by DNS for Q = 2 L/min, ω = 1000 rpm with a film thickness of 500 µm.

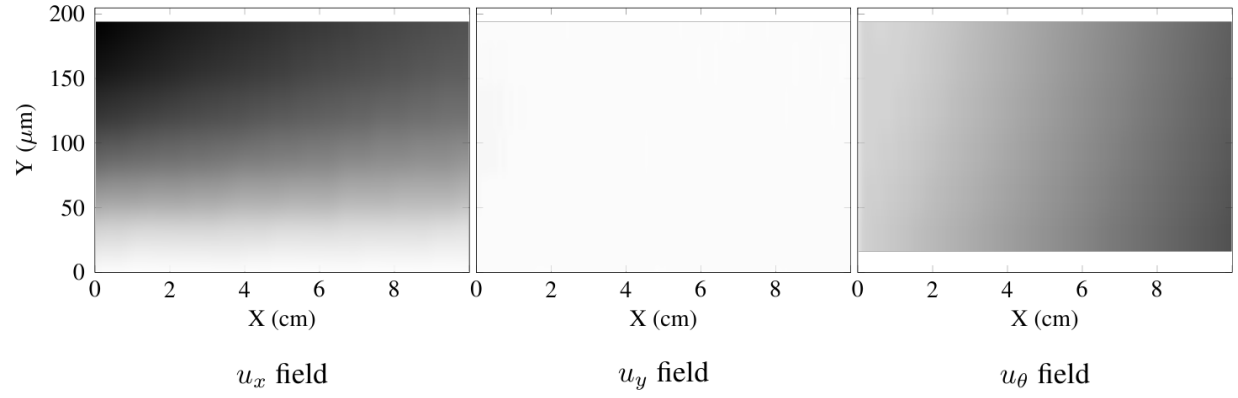

Figure 3: Flow field computed by DNS for Q = 2 L/min, ω = 1000 rpm with a film thickness of 200 µm.

Knowledge of the film thickness allows us in our modelling to impose proper slip conditions at the air/water interface due to the high ratio between the respective viscosities of the two phases. With such conditions, the flow velocity profile calculated by DNS matches the hypothesised flow field already reported by Kroll-Rabotin et al. (2010): a parabolic profile in the streamwise direction (*x* direction in Figure 1) that can be scaled with respect to film thickness and a solid body rotation in the azimuthal direction.

In Figures 2 or 3, we observe that the flow is fully developed and predictable almost immediately after the film inlet and that the velocity profile stays the same along the entire bowl length. Moreover, this observation does not depend on the velocity profile one may choose at the inlet of

the film. Consequently, it is not necessary to account for any effect that the impeller may have on the flow field at the film inlet: the role of the impeller is limited to giving the fluid a high enough initial velocity to avoid filling up the bowl.

As shown by Makarytchev et al. (1997), the film undergoes continuous thinning over the bowl length. However, this thinning has no effect on the velocity profile in the y-direction; hence it is sound to assume a constant thickness over the bowl length in the model. Following the analytical law given by Makarytchev et al. (1997), the ratio between inlet and outlet thickness is $(1 + L/R_0 \sin(\beta/2))^{-2/3}$ which is higher than 0.8 with a Falcon L40. In the end, we use a constant film thickness equal to that calculated by DNS.

Criterion for Particle Capture

Since every particle that enters the bed is captured, prediction of separation boils down to predicting particle trajectories inside the film. Depending on the solution that may be used to solve the transport problem, we quantify separation either from the trajectories that intersect the bowl surface (which yields recovery to the heavy stream) or those that intersect the outlet film boundary (which yields recovery to the light stream).

The trajectory of any given particle depends on its density and size, its initial distance to the wall (Y_0) at the film inlet and the operating conditions of the Falcon. Each particle follows a specific trajectory through the liquid film, until it either hits the bowl or it reaches the end of the film and exits the bowl. We refer to the distance between the film inlet and the point at which the particle hits the wall as the sedimentation length (see Figure 1). Comparing this sedimentation length to the actual bowl length yields an objective criterion for particle capture.

In order to compute particle recovery to concentrate (C_p) from the trajectory-based capture criterion, we must quantify the fraction of particles whose sedimentation length is less than the bowl length, or alternatively the fraction of particle whose sedimentation length is greater than the bowl length.

We assume that the four blade propeller mixes the feed particles homogeneously at the inlet of the film. In other words, the distribution of particles is assumed to be uniform across the whole film thickness at the film inlet. This uniform distribution implies that the flux of particles that enter the film at elevation Y_0 inside the film is directly proportional to the fluid velocity profile at the same elevation. By combining feed washability and particle trajectory predictions, concentrate and tailings washabilities can be predicted, along with the Falcon partition function.

Particle Trajectories in the Liquid Film

Force Balance

The criterion of capture is based on the particle trajectories moving through the flowing film. More precisely, we need to predict the trajectory of the ultimate particle reaching the bowl outlet. These trajectories can be calculated by integration of Newton's second law (Equation 1) with

forces given in Equations (2a), (2b), (2c) and (2d).

$$\rho_p \mathcal{V}_p \frac{\mathrm{d}\vec{v}}{\mathrm{d}t} = \sum \vec{F} \tag{1}$$

The forces experienced by moving particles (volume V_p) within the flowing film (Clift et al., 1978) are:

- buoyancy (Equation 2a) which is due to density difference between the solid particles (ρ_p) and the fluid (ρ_f) under the action of gravity (g),
- the effect of pressure gradient (Equation 2b),
- the added mass force (Equation 2c) due to inertia of the fluid either due to flow or particle acceleration,
- the drag force (Equation 2d) which accounts for pressure and viscous contributions.

$$\vec{F}_B = (\rho_p - \rho_f)\, \mathcal{V}_p\, \vec{g} \tag{2a}$$

$$\vec{F}_G = \rho_f \mathcal{V}_p \frac{\mathrm{D}\vec{u}}{\mathrm{D}t} \tag{2b}$$

$$\vec{F}_M = \rho_f \mathcal{V}_p C_M \left(\frac{\mathrm{D}\vec{u}}{\mathrm{D}t} - \frac{\mathrm{d}\vec{v}}{\mathrm{d}t} \right) \tag{2c}$$

$$\vec{F}_D = \frac{1}{2}\, \rho_f \mathcal{S}_p C_D\, |\vec{u} - \vec{v}|\, (\vec{u} - \vec{v}) \tag{2d}$$

Forces F_G, F_M and F_D depend on the fluid velocity (u) at the particle position and on spatial gradients (Du/Dt). The added-mass coefficient $C_M = 1/2$ while C_D depends on the particulate Reynolds number. We have neglected the history and lift forces.

Analytic Scaling Law

An estimate of the particle velocity can be obtained neglecting the particle slip velocity along the main flow direction and simply balancing drag and centrifugal forces (Kroll et al., 2010). Using Stokes drag law the settling velocity normal to the wall is calculated and yields a theoretical prediction of the settling length along the bowl wall (Equations 3a and 3b).

$$L^{1+\alpha} \propto \frac{9}{4\pi} Q\, \omega^{-2}\, r_p^{-2}\, (\rho_p - \rho_f)^{-1}\, \mu\, R_0^{-2+\alpha} \left(\cos \frac{\beta}{2} \right)^{-1} \tag{3a}$$

$$\alpha = \frac{\ln \left(1 + \frac{L}{R_0} \sin \frac{\beta}{2} \right)}{\ln \frac{L}{R_0}} \tag{3b}$$

In this expression, the operating conditions of the bowl fix the flow rate (Q) and its spinning rate (ω). Regarding the particle properties, we need to know the particle radius (r_p) and its density

(ρ_p), while the properties characterizing carrying fluid are its dynamic viscosity (μ) and its density (ρ_f). The bowl geometrical characteristics are its base radius (R_0) and the cone angle (β). Since this expression is based on Stokes drag law the estimate of the settling speed is only valid for low particulate Reynolds numbers (Re_p < 1). Thanks to Equation (4), it is possible to determine the range of validity of these assumptions for given operating conditions.

$$Re_p \approx \frac{4}{9}\left(\frac{\rho_p}{\rho_f} - 1\right)\frac{\omega^2 r_p^3 R}{\nu^2} \tag{4}$$

Under such conditions, the captured fraction of solids in the bowl for each particle type (C_p) is:

$$C_p = \min\left(\frac{4\pi}{9} Q^{-1}\,\omega^2\,\Delta\rho\, r_p^2\,\mu^{-1}\,R_0^{2-\alpha}\,\cos\frac{\beta}{2}\,L_{\text{bowl}}^{1+\alpha},\ 1\right) \tag{5}$$

Therefore, the feed fraction captured in the bowl (C) depends on the washability l_{feed} through Equation (6).

$$C = \iint l_{\text{feed}}(r_p, \rho_p)\, C_p(r_p, \rho_p)\mathrm{d}r_p\,\mathrm{d}\rho_p \tag{6}$$

Numerical Solution of Trajectories

When the particulate Reynolds number is moderate or large (Re_p > 1), the drag force is no longer linear with the particle velocity. Analytic estimate of the particle velocity is not possible leading to numerical simulation of Equations (1) and (2) for particle trajectory. The drag coefficient can be approximated by the empirical law of Schiller and Naumann (1935) (Equation 7).

$$C_D = \frac{24}{Re_p}\left(1 + 0.15 Re_p^{0.687}\right) \tag{7}$$

Trajectories are then computed by numerical integration of the force balance over time. Trajectories yield particle sedimentation lengths related to their initial position across the film thickness. So, it is straightforward to locate the initial position verifying the capture criterion and consequently to compute the captured fraction of each particle type (C_p). This has been extensively described in our former paper (Kroll-Rabotin et al., 2010).

APPLICATION OF THE MODEL TO ULTRAFINE SUSPENSIONS

From the industrial point of view, the reduction of water consumption is a major concern in physical separation processes. Using the Falcon UF concentrator without internal fluidization flow is a major asset: water is only used as the carrier fluid in feeding suspension. The effect of

suspension volumetric concentration may be a key operating parameter for real applications of the Falcon UF concentrator. However, in our former modelling of particle Lagrangian trajectories, the assumption of isolated particle leads to non-interacting trajectories. This is flawed when the concentration is moderate or high while particle/particle hydrodynamic interactions will couple all the trajectories. The actual particle settling speed depends on the local solid fraction through a hindered correction factor. The separation process acting inside the Falcon bowl induces a variation of particle concentration along the bowl length and the bulk properties of the suspension. The model for concentrate suspensions must account for spatial variations of the volumetric concentration of the suspension within the fluid film.

Effect of the Local Concentration of the Suspension

The temporal evolution of the volumetric fraction (φ) of each particle type can be computed by accounting convective fluxes of particles through a closed surface S delimiting a finite volume V (Equation 8). The local variation of the particle velocity field (v) has to be modelled for each particle type. Due to hindrance effect (v) is a function of the concentration. Although we investigate the separation of ultrafine particles, their typical size does not fall below 1 µm. Diffusion due to Brownian agitation can be neglected.

$$-\frac{\mathrm{d}\phi}{\mathrm{d}t} = \frac{1}{\mathcal{V}} \oint_{\mathcal{S}} \phi \vec{v} \cdot \mathrm{d}\vec{\mathcal{S}} \tag{8}$$

Numerical Approach

Due to rotation symmetry, the evolution of concentration in the azimuthal direction does not need to be solved. The fluid film is finely discretized along its thickness and along the bowl length. The number of cells along bowl length is "n_i" while we note the number of cells across the film thickness "n_j". Volumetric fractions of particles for each size and density composing the washability of the sediment are computed simultaneously in all cells within the film. The washability is also discretized through the range of density and size of the suspension that we investigate. Particles are transported by the fluid film at high speed and cells dimension are small, so the particle residence time inside in each cell is very short ($t_s \approx 2\pi rhL/(Q\ ni)$) compared to the operating time scales of the separation (cycle time, filling time of the retention zone). Therefore, it is relevant to use an Eulerian modelling for predicting the mean quantities such as the evolution of the local concentration although mesh cell size might be in some cases comparable or smaller than the typical particle size.

Finite volumes method

The film is divided into annular cells (see Figure 4) whose rectangular cross sections have indices i along the wall direction and j across the thickness. Equation (8) yields the sum of fluxes through all 4 faces.

$$-\frac{\mathrm{d}\phi_{i,j}}{\mathrm{d}t} = \frac{1}{\mathcal{V}_{i,j}} \left(K_{i,j+1/2}\phi_{i,j+1/2} - K_{i,j-1/2}\phi_{i,j-1/2} + K_{i+1/2,j}\phi_{i+1/2,j} - K_{i-1/2,j}\phi_{i-1/2,j} \right) \tag{9}$$

The coefficients $K_{i,j}$ are functions of the local particle velocity inside each cell.

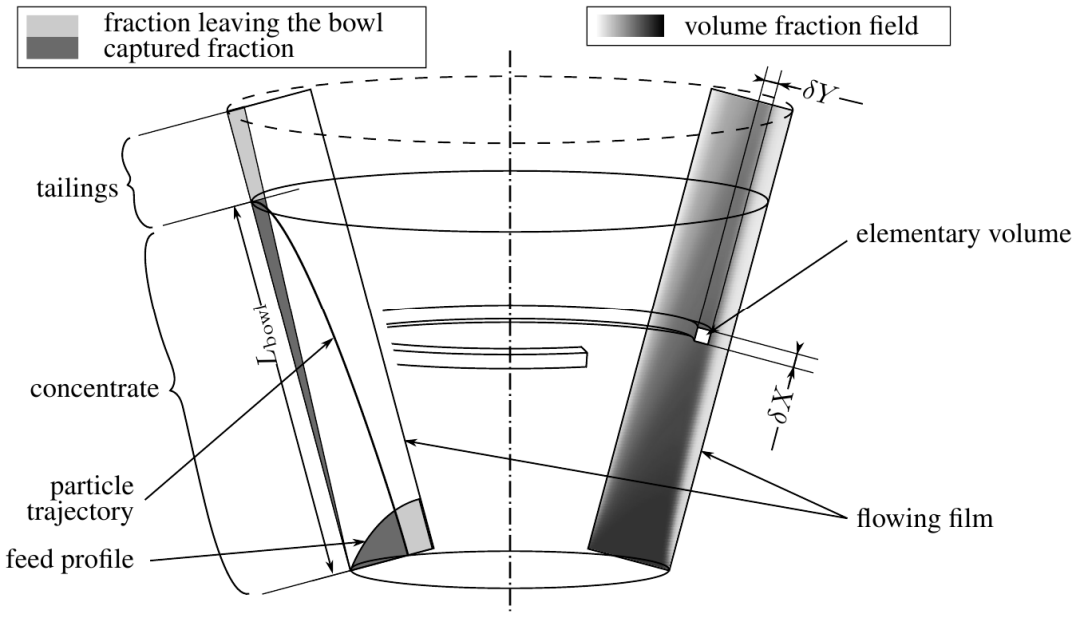

Figure 4: Two numerical approaches for predicting particle capture: Lagrangian tracking in the film (used with the dilute model) and volume fraction computation in the film (used with the concentrated model).

Boundary conditions

On the inlet section ($i = 1$), the fraction of each particle type is imposed according to the composition of the processed suspension washability. At the water/air interface ($j = n_j$), solid fluxes through this boundary are null (no particle is crossing the upper surface of the film). In the outlet section of the bowl ($i = n_i$), a numerical boundary condition models the free exit of the suspension. We assume that the longitudinal concentration gradient is zero at the outlet. At the bowl wall, all the particles reaching the bed are captured. This means that they are withdrawn from the computation domain when they reach the solid bed at the wall. The bed dynamics is not simulated and is taken into account by an outlet boundary condition (perfect sink).

Boundary conditions in $i = n_i$, $j = 1$ and $j = n_j$ corresponds to imposed fluxes which are directly used in Equation (9) while the boundary condition at $i = 1$ is a fixed concentration.

Steady state solution

We are interested in the steady state solution because the transient evolution of the concentration in the film is likely to be very short compared to the bed loading. The centrifugal settling time of the particles toward the wall is very short compared to process operating time scales. Therefore, we only seek solutions of Equation (9) at steady state.

Using the boundary conditions, the finite volumes method yields a system of algebraic equations (10).

$$\forall j \in [1, n_j], \quad \phi_{1,j} = \phi^0_{1,j} \tag{10}$$
$$\forall i \in [2, n_i],\ \forall j \in [1, n_j],$$
$$K_{i,j+1/2}\phi_{i,j+1/2} - K_{i,j-1/2}\phi_{i,j-1/2} + K_{i+1/2,j}\phi_{i+1/2,j} - K_{i-1/2,j}\phi_{i-1/2,j} = 0$$

The concentration field in the whole film can then by computed by solving simultaneously all the equations of the system provided that we know the particle velocity field. For dilute system, the system is linear and becomes non-linear when including hindrance effects.

The Particle Velocity

Neglecting particle inertia on the left hand side of Equation (1), we consider that particles are moving with a constant slip velocity given by the balance between the drag and the other forces.

$$\sum \vec{F} = 0 \tag{11}$$

The hypothesis that the inertial contribution can be neglected is valid for low Stokes numbers which quantifies the ratio between viscous particulate relaxation time of particles and the fluid flow time scales. Indeed, the assumption has been tested a posteriori with our simulation results. It is confirmed that for the case of ultrafine suspensions (< 80 μm) composed of low density solid fractions (s.g.< 3), the inertial contribution to the particle trajectory is minor: it only affects particle corresponding to ratio to product equal to 100%.

Neglecting particle inertia, the velocity field of the particles depends only on local physical properties of the suspension. It is possible to compute the particle settling velocity field (v) to be used in the linear system (Equation 10).

In addition, as particulate interactions become significant, other contributions supplement the force balance (Equation 2). The explicit computation of the settling velocity of particles towards the wall requires an empirical expression relating the local properties of the suspension to hindrance effect.

The method we used has been proposed by Concha and Bürger (Bürger et al., 2000; Concha and Bürger, 2002). It consists in using a hindered settling law that fits monodisperse suspension behaviour for each particle types. Meanwhile, the effect of solid concentration is accounted for in the bulk viscosity and density of the suspension (continuous medium approach). The back flow in the fluid due to particulate flux is also accounted for. We use the hindered settling law from Concha and Almendra (1979), the suspension viscosity law from Krieger and Dougherty (1959) and the bulk density is defined as the average density of water and all particle types, weighted by their respective volume fractions (Equation 12d).

In all cells of the simulation, we compute Equations (12).

$$\vec{v}_p - \vec{u}_s = \vec{v}_{\mathrm{C\&A}}\left(r_p, \rho_p, \rho_s, \mu_s, \omega^2\vec{r}, \textstyle\sum_p \phi_p\right) \quad \text{Concha \& Almendra (1979)} \quad (12a)$$

$$\vec{u}_s = \vec{u} - \frac{\sum_p \vec{v}_{\mathrm{C\&A,p}}\,\phi_p}{1 - \sum_p \phi_p} \quad \text{Burger et al (2000)} \quad (12b)$$

$$\mu_s = \mu\left(1 - \frac{1}{\phi_{\max}}\sum_p \phi_p\right)^{-[\eta]\phi_{\max}} \quad \text{Krieger and Dougherty (1959)} \quad (12c)$$

$$\rho_s = \left(1 - \sum_p \phi_p\right)\rho_f + \sum_p \phi_p \rho_p \quad (12d)$$

Using the model for dilute suspensions, these properties are always those of the carrying fluid, whereas in concentrate suspension, the whole feed washability has an impact on the results.

Equation (12c) needs two empirical parameters φ_{max} and [η]. Einstein (1956) showed that [η] is 5/2 for hard spheres if the particle volume fraction remains low (typically less than 5%). φ_{max} is the maximum volume fraction at close packing. For monodisperse hard spheres, this value is around $\varphi_{max} \approx 0.63$ (McGeary, 1961). In our case, suspensions are composed of polydisperse particles (the size ratio ranging typically between 1 and 200). Small particles are able to fill open spaces between larger ones leading to $\varphi_{max} \approx 1$. We used the value $\varphi_{max} = 0.8$ because above this value the viscosity evolution law (Equation 12c) for larger φ_{max} has a minor effect on the bulk viscosity over the range of our investigation (concentration from 0% to 40%).

Model Resolution

Since particle settling velocity depends on the local properties of the suspension in the film through the solid fraction φ_p, equation (12a) is non-linear and an iterative numerical method is used in order to calculate the fully developed steady-state flow field. Figures 4 and 8 give examples of concentration profiles that are calculated inside the film. In the end, the concentration of each particle type inside the $n_i \times n_j$ discrete cells that are used to mesh the film is calculated. Separation is evaluated by direct summation of the concentration profile in the n_i cells that mesh the outlet of the film.

MODEL VALIDATION

In this section, we first validate the key model hypotheses we discussed through a number of well-chosen laboratory tests with a Falcon L40 separator. We then discuss the Falcon's ability to separate ultrafine particles by interrogating the model using the washability of dredged sediments. It is worth pointing out that dredged sediments are low-density materials, with particle specific gravity ranging between organic materials and quartz. In passing, we note that

the size and density range in question overlaps with that of fine coal tailings.

Laboratory-Scale Experiments

Model validation testwork was done with a suspension of silica particles. From their chemical analysis (Table 1), the particles can be considered to have a single density, hence the washability of the suspension is only a function of particle size distribution. Characteristic sizes of the particle size distribution, which was measured with a Malvern Mastersizer 2000, are d_{10} = 3 μm, d_{50} = 17 μm and d_{90} = 46 μm.

Table 1: Chemical analysis (in oxides) of the silica particles used in the experiments.

SiO_2	> 98.5 %
Fe_2O_3	< 450 ppm
Al_2O_3	< 7500 ppm
TiO_2	< 360 ppm
CaO	< 300 ppm
K_2O	< 5500 ppm

The L40 concentrator is a semi-batch apparatus. The tailings (light) stream exits the separator continuously and can be sampled over time. The concentrate (heavy) stream can only be analysed at the end of the experiment. Hence, data reconciliation is necessary to calculate the separation efficiency under any given conditions. Full analysis of performance requires that the Falcon be stopped. The concentrator is operated at a constant flow rate and the size distribution and concentration of the feed is constant throughout the experiment.

Experimental Confirmation of the No-Resuspension Hypothesis

The key hypothesis of the model is that particles are captured when they reach the bowl wall, meaning that they cannot be resuspended once captured. In a semi-batch Falcon concentrator such as the L40, it is well-known that the particle bed volume increases over time until it fills up the retention zone completely, which triggers a sharp drop in separation efficiency (Laplante et al., 1994; Laplante and Nickoletopoulos, 1997). What we need to ascertain here is whether the entire feed stream exits through the overflow once the bed occupies the retention zone as per our no-resuspension hypothesis. In order to validate this hypothesis, we measured the size distribution in the tailings over a long enough time for the drop in separation efficiency to occur. Figure 5 shows the evolution of the particle size distribution in the overflow as a function of time under test conditions Q = 4.42 L/min and ω = 1460 rpm. For the first couple of minutes (108 seconds) in this experiment, we find that the size distribution of the overflow is invariant. This means that separation efficiency is constant during this period. Beyond this time, the size distribution changes rapidly, up to a point where it resembles the size distribution of the feed. At this point, the retention zone of the Falcon concentrator is full and no separation occurs at all. The invariance of the size distribution of the overflow stream during the first couple of minutes

proves that the state of filling of the retention zone has no effect on the separation efficiency. The experimental demonstration that there is not any measurable resuspension of captured particles during normal operation of the Falcon concentrator validates our model and the assumptions that underlie the analytical scaling law we derived for dilute suspension.

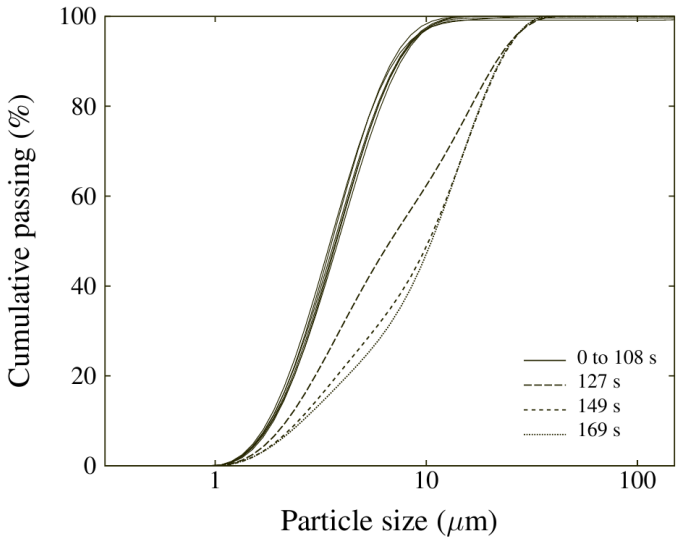

Figure 5: Measured time variation of the particle size distribution for the overflow (Q = 4.42 L/min, ω = 1460 rpm).

Validation of the Scaling Law for Dilute Suspensions

Solids concentration in the overflow was measured for different operating conditions, and compared to predictions using the scaling law. Figure 6 shows that predictions are in remarkable agreement with the measured data. Indeed, the solid lines in Figure 6 correspond to scaling law predictions using Equation (6) corrected only with a constant coefficient of 0.66 (so the constant part of Equation 5 becomes $0.66 \times 4\,\pi / 9$).. What this means is that the the model that we derived captures all the key aspects of the physics that govern particle transport inside a Falcon concentrator. A key strength of the scaling law is that it gives a clear and direct understanding of the relative significance of all the process parameters on separation efficiency. However, the validity of the scaling law is limited to dilute suspensions and concentration effects should be accounted for using the concentrated model in order to handle industrial situations with high solids concentrations.

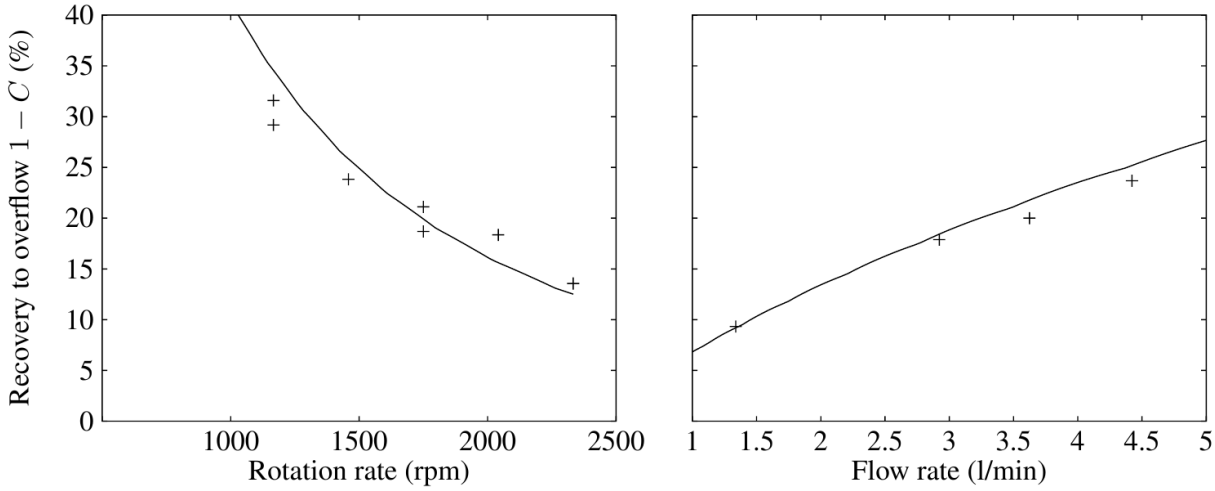

Figure 6: Comparison between scaling law predictions and experimental data with dilute silica suspensions (varying rotation rate with Q = 4.5 L/min and varying flow rate with ω = 1460 rpm, both experiments were run at 1.2 wt% solid with silica suspension of d_{50} = 17 µm).

Model Application to Ultrafines Beneficiation

Applications of Falcon concentrators with ultrafine low specific gravity suspensions, for which our model is validated, can be found in the literature. In particular, Honaker and co-workers did use a Falcon concentrator for fine coal beneficiation (Honaker et al., 1996; Honaker and Wang, 1998; Honaker and Patil, 2002). The situation that we are interested in concerns the beneficiation of fine dredged sediments. Such sediments contain a mixture of organic matter and sand particles, and its rather unique washability is given in Figure 7. As the pollution tends to report to the finer size fractions, our objective is to test the ability of the Falcon concentrator to separate the organic fraction from the sand fraction at a size about 10 µm, in order to produce a valuable +10 micron sand fraction.

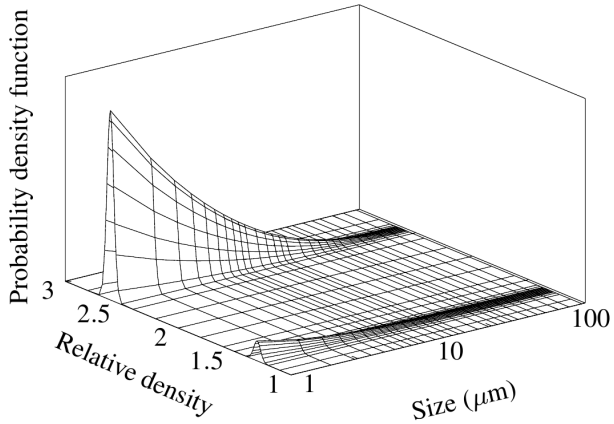

Figure 7: Washability of the dredged sediments used in this work.

Concentration Effect

When particles with different densities are mixed, the way by which each particle type affects the flow, or is affected by the flow, differs. Low-density particles have little effect on the overall suspension density, but when suspension density varies locally, their trajectories are impacted significantly. Indeed, scaling law (Equation 3, for example) shows that particles are more or less affected depending on their density difference with the carrying fluid: the smaller the density differential, the more sensitive particles become to suspension density variations. Conversely, denser particles are less sensitive to variations in suspension density due to their higher density differential with the fluid, but they have an important impact on the density of the suspension in their immediate neighbourhood. In regions where they are present in high concentration, they can yield a local density high enough to prevent settling of less dense particles. Hence, increasing solid fraction in the feed increases local concentration effects depending on feed washability, which can possibly help separate particles on the basis of their specific gravity. This beneficial effect is expected to apply up to a point.

Moreover, each particle travelling in the film displaces an equivalent volume of fluid in a direction opposite to its direction of motion. In regions where particles settle rapidly, the resulting back-flow of fluid becomes significant and can potentially prevents settling of particles with lower settling velocity. This back-flow effect is likely to contribute to differential settling, which is the main separation mechanism inside a Falcon concentrator.

Figure 8 shows the concentration distribution of a given particle type. It illustrates the improvement in particle separation that results from the concentration effects discussed previously. Indeed, Figure 8 clearly shows two regions: a lower region that contains most of the particle of the type considered, and a region above with a lesser concentration. The particle type whose volume fraction field is shown in Figure 8 belongs to the low density fraction of a suspension that is bimodal in density. Figure 8 clearly shows the back-flow effect caused by settling of the denser particles, which lift the low density fraction in the higher region. We see that the lighter fraction settles to the right of Figure 8, that is after the denser particles have already settled.

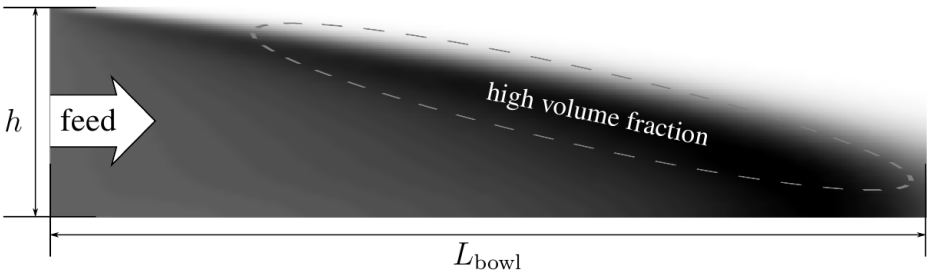

Figure 8: Concentration variations for a lighter particle type in a suspension combining two materials of different densities.

The model also predicts that increasing the fraction of denser particles will increase the sedimentation length of less dense particles. Since particle capture is dictated by sedimentation

length, increasing solid fraction can possibly improve separation of light organic particles from heavier sand particles. Of course, whether this effect plays a significant effect or not will depend on the washability of the feed material and the operating conditions. The value of modelling as a guide for identifying the favourable sets of conditions is self-explanatory.

Application to Beneficiation of Dredged Sediments

As indicated earlier, our research is concerned with beneficiating dredged sediments by separating the +10 micron sand fraction from the lighter organic fraction and the -10 micron sand particles. Therefore, we have applied our concentrated model to an actual washability for dredged sediments. Figures 9 and 10 show predicted grade-recovery curves for our laboratory UF bowl (diam. 10 cm). Starting with a feed that contains 11 wt% organics, the model behaves as expected, i.e. organics recovery increases with the recovery to concentrate. Figure 9 predicts that increasing feed solids concentration up to 30.5 vol% is beneficial to the process. As indicated earlier, this finding cannot be generalised as it is the result of the combination between the washability of the feed and the operating conditions of the Falcon. Figure 8 also includes predictions using two flowrates, the larger one being almost double the first one. The predicted effect with the concentrated model is that the values of recovery are close, and that they sit on a single grade-recovery curve that does not depend on feed rate. As already known from the scaling law, rotation velocity has a strong effect on recovery. This is perhaps best appreciated in Figure 10. For practical purposes, Figure 10 is very useful as it gives a direct prediction of the maximum sand recovery as a function of organics recovery. More detailed analysis of model predictions can be done for process optimisation, such as with size-by-size recovery analysis. All in all, model predictions indicate that the Falcon concentrator is a promising separator for beneficiation of dredged sediments. Indeed, with the sample sediment whose washability we used, one pass through the UF bowl removes half of the organic fraction in mass. Process optimisation calculations are necessary in order to identify the best set of conditions for beneficiating this particular dredged sediment.

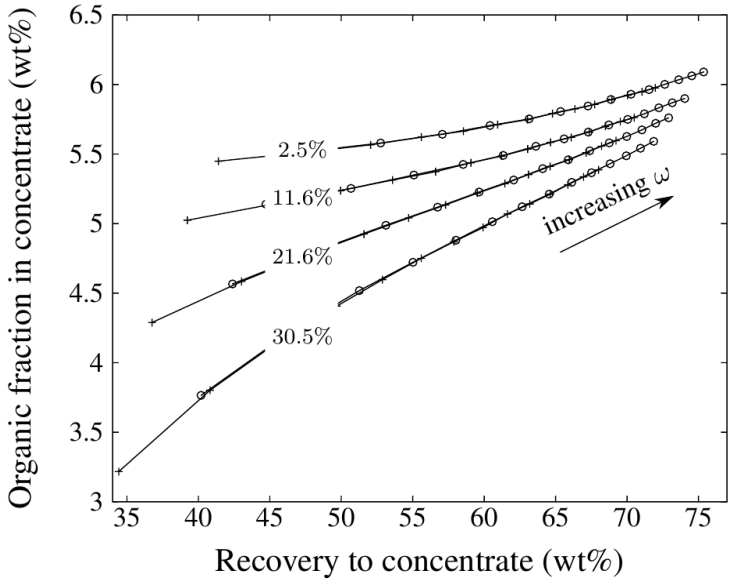

Figure 9: Grade-recovery curves as a function of solids concentration. The feed contains 11wt% organics. Separation is predicted for a Falcon L40 operating at 3 L/min (o) and 5 L/min (+).

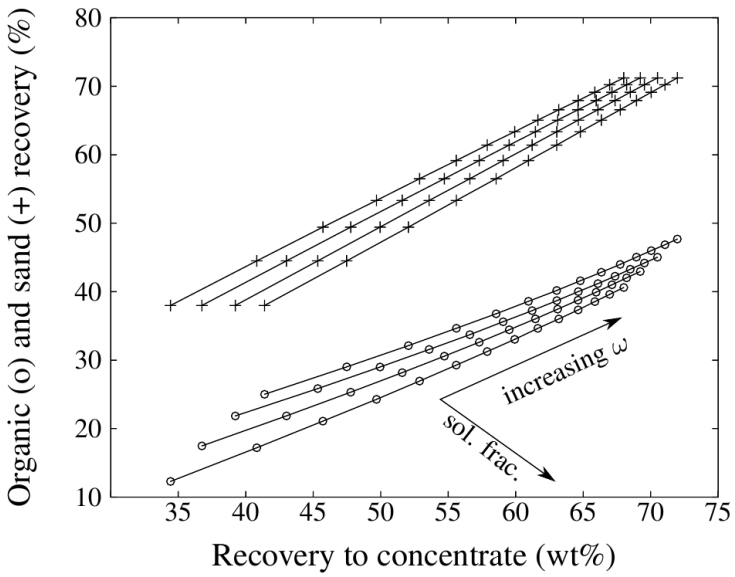

Figure 10: Recovery predictions for dredged sediments, showing the effect of feed solids concentration and rotation velocity.

CONCLUSIONS AND PERSPECTIVES

In this paper, we have presented the mechanistic model we developed for the UF Falcon separator and validated its key hypotheses. Our objective is to quantify its potential for beneficiation of ultrafine low-density (s.g. < 3) suspensions made of dredged sediments. The gravity separation challenge with dredged sediments comes mainly from the particle size of the material, whose valuable sand fraction is in the 100 μm × 10 μm particle size range. Particle fineness, along with the relatively high concentration of valuable material in the feed, make this problem quite different from standard Falcon applications.

Under dilute conditions, our model leads to an interesting analytical solution. In addition to providing us with valuable insights about the relative significance of the process variables on separation efficiency, this model was used to test the validity of the physics used to model the UF Falcon concentrator.

We then extended the model to the case of concentrated suspensions, which can no longer be solved analytically. With the latter model, we showed that increasing concentration can be beneficial to separation efficiency under some conditions. This is a rather interesting finding that needs to be verified experimentally, and experiments with concentrated suspensions are being planned for validating the extended model.

Finally, optimization work with the proposed model is underway for identification of the best set of conditions that are required to beneficiate ultrafine dredged sediments with the UF Falcon concentrator. Already mentioned in the paper, the washability of dredged sediments resembles that of fine coal tailings, and we are already planning to use the model for testing the possibility

of beneficiating fine coal tailings with a UF Falcon concentrator.

ACKNOWLEDGEMENTS

This work is funded by the French "Agence Nationale pour la Recherche" (ANR), in the framework of the PRECODD-PROPSED project.

REFERENCES

Bürger, R., Concha, F., Fjelde, K.-K., and Hvistendahl Karlsen, K. (2000). Numerical simulation of the settling of polydisperse suspensions of spheres. *Powder Technology*, 113:77–318.

Clift, R., Grace, J. R., and Weber, M. E. (1978). Bubbles, Drops and Particles. Academic Press.

Concha, F. and Almendra, E. R. (1979). Settling velocities of particulate systems, 2. settling velocities of suspensions of spherical particles. International *Journal of Mineral Processing*, 6:31–41.

Concha, F. and Bürger, R. (2002). A century of research in sedimentation and thickening. *Kona: powder and particle journal*, 20:38–69.

Deveau, C. (2006). Improving fine particle gravity recovery through equipment behavior modification. In *Proceedings of the 38th Annual Meeting of the Canadian Mineral Processors*, Paper 31, pages 501–517.

Deveau, C. and Young, S. R. (2005). Pushing the limits of gravity separation. In *Proceedings of the Society for Mining, Metallurgy and Exploration Annual Meeting*.

Einstein, A. (1956). Investigations on the Theory of Brownian Movement. New York: Dover.

Honaker, R. Q. and Patil, D. P. (2002). Parametric evaluation of a dense-medium process using an enhanced gravity separator. *Coal Preparation*, 22(1):1–17.

Honaker, R. Q. and Wang, D. (1998). Falcon concentrators: a high capacity fine coal cleaning technology. In *Proceedings of the Society for Mining, Metallurgy and Exploration Annual Meeting.*

Honaker, R. Q., Wang, D., and Ho, K. (1996). Application of the Falcon concentrator for fine coal cleaning. *Minerals Engineering*, 9(11):1143–1156.

Krieger, I. M. and Dougherty, T. J. (1959). A mechanism for non-Newtonian flow in suspensions of rigid spheres. *Journal of Rheology*, 3(1):137–152.

Kroll-Rabotin, J.-S., Bourgeois, F., and Climent, E. (2010). Fluid dynamics based modelling of the Falcon concentrator for ultrafine particle beneficiation. *Minerals Engineering*, 23(4):313–

320. Special Issue: Physical Separation.

Laplante, A. R., Buonvino, M., Veltmeyer, A., Robitaille, J., and Naud, G. (1994). A study of the Falcon concentrator. *Canadian Metallurgical Quarterly*, 33(4):279–288.

Laplante, A. R. and Nickoletopoulos, N. (1997). Validation of a Falcon model with a synthetic ore. *Canadian Metallurgical Quarterly*, 36(1):7–13.

Makarytchev, S. V., Xue, E. , Langrish, T. A. G., and Prince, R. G. H. (1997). On modelling fluid flow over a rotating conical surface. *Chemical Engineering Science*, 52:1055–1057.

McAlister, S. A. and Armstrong, K. C. (1998). Development of the Falcon concentrator. In *Proceedings of the Society for Mining, Metallurgy and Exploration Annual Meeting.*

McGeary, R. K. (1961). Mechanical packing of spherical particles. *Journal of the American Ceramic Society*, 44:513–522.

Schiller, L. and Naumann, Z. (1935). A drag coefficient correlation. *Zeitschrift des Vereines Deutscher Ingenieure*, pages 77–318.